Ann. Geophys., 26, 1479–1490, 2008
www.ann-geophys.net/26/1479/2008/


Annales Geophysicae

# Space weather effects on radio propagation: study of the CEDAR, GEM and ISTP storm events

**D. V. Blagoveshchensky**[1], **A. S. Kalishin**[2], **and M. A. Sergeyeva**[1]

[1]University of Aerospace Instrumentation, 67, Bolshaya Morskaya, St. Petersburg, 190000, Russia
[2]Arctic and Antarctic Research Institute, 38, Bering Street, St. Petersburg, 199397, Russia

Received: 2 August 2007 – Revised: 18 February 2008 – Accepted: 14 March 2008 – Published: 11 June 2008

**Abstract.** The impact of 14 geomagnetic storms from a list of CEDAR, GEM and ISTP storms, that occurred during 1997–1999, on radio propagation conditions has been investigated. The propagation conditions were estimated through variations of the MOF and LOF (the maximum and lowest operation frequencies) on three high-latitude HF radio paths in north-west Russia. Geophysical data of $D_{st}$, $B_z$, AE as well as some riometer data from Sodankyla observatory, Finland, were used for the analysis. It was shown that the storm impact on the ionosphere and radio propagation for each storm has an individual character. Nevertheless, there are common patterns in variation of the propagation parameters for all storms. Thus, the frequency range $\Delta$=MOF−LOF increases several hours before a storm, then it narrows sharply during the storm, and expands again several hours after the end of the storm. This regular behaviour should be useful for the HF radio propagation predictions and frequency management at high latitudes. On the trans-auroral radio path, the time interval when the signal is lost through a storm ($t_{\mathrm{des}}$) depends on the local time. For the day-time storms an average value $t_{\mathrm{des}}$ is 6 h, but for night storms $t_{\mathrm{des}}$ is only 2 h. The ionization increase in the F2 layer before storm onset is 3.5 h during the day-time and 2.4 h at night. Mechanisms to explain the observed variations are discussed including some novel possibilities involving energy input through the cusp.

**Keywords.** Ionosphere (Polar ionosphere) – Magnetospheric physics (Storms and substorms) – Radio science (Ionospheric propagation)

*Correspondence to:* D. V. Blagoveshchensky
(dvb@ppp.delfa.net)

## 1 Introduction

Space weather is known to have a significant impact on human activity on the Earth (Buonsanto, 1999; Gonzales et al., 1994; Galeyev et al., 1996; Baker, 1996; Lastovicka, 2002). It affects both spacecraft (satellites and vehicles), and impacts various ground-based services and systems (communication, radars, navigations). Very intense geomagnetic disturbances, storms, are rare, but their space-weather effects can lead to catastrophic consequences. Thus it is very important to understand the physical mechanisms of these disturbances, so that forecasting can be more reliable and appropriate mitigation and adaption strategies adopted.

Blagoveshchensky et al. (1992, 1996, 2000, 2003, 2006) determined the impact of moderate geomagnetic substorms ($AE_{max}$=100–600 nT) on the ionosphere and HF radio propagation on mid-latitude and subpolar radio paths. This paper presents the analysis of the impact of intense geomagnetic storms ($AE_{max}$=800–2000 nT) on HF radio propagation at high latitudes on several high latitude HF radio paths in north-west Russia. It utilizes geomagnetic storms from a list of CEDAR, GEM and ISTP storms, from 1997–1999. The impact of the storms is estimated from the variations of the operational frequency range MOF-LOF (the maximum and lowest observed frequencies) on each path before, during and after a magnetospheric storm. Identifying repeatable behaviour is essential for predicting more accurately HF radio propagation conditions in polar and subpolar regions. The physical mechanisms of disturbance impact on radio propagation are considered. In this study we do not address the high-latitude effects associated with patches, blobs, and the main ionospheric trough. These effects have been considered in other papers, for instance (Goodman and Ballard, 2004; Warrington and Stocker, 2003; Hunsucker and Hargreaves, 2003).

Published by Copernicus Publications on behalf of the European Geosciences Union.

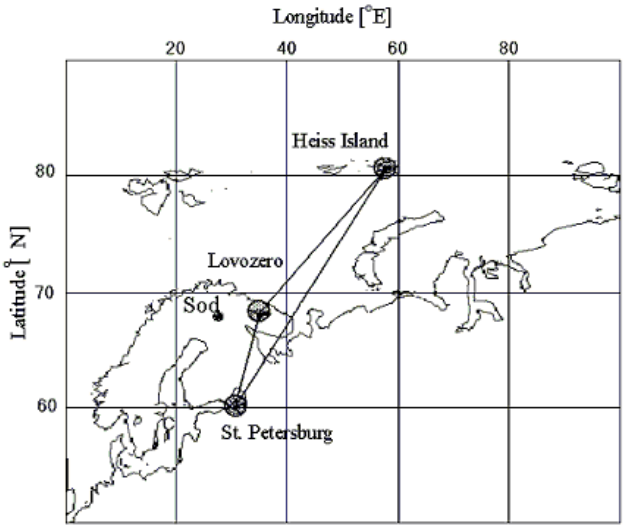


**Fig. 1.** The system of radio paths. The subauroral St. Petersburg-Lovozero path has the midpoint inside the main ionospheric trough for quiet conditions. The transauroral St. Petersburg-Heiss Island path has the midpoint inside the auroral oval. The polar-auroral Lovozero-Heiss Island path has the midpoint on the border of the oval and the polar cap. Here is also location of Sodankyla observatory.

## 2 Operational techniques

The experimental HF radio path system is presented in Fig. 1.

For the first path, the transmitter is at St. Petersburg and the receiver is 1000 km distant at Lovozero. The midpoint is located on geomagnetic latitude $\Phi'$=61°. As a result, under normal geomagnetic conditions, this is a subauroral path. The midpoint of the path lies inside the main ionospheric trough (MIT), close to the polar edge of the trough, under quiet geomagnetic conditions. During a magnetospheric storm, the polar edge of the trough (PET) moves toward the equator, and the midpoint of the path is most likely then in the boundary of diffuse precipitation (BDP) region. This is true in darkness but not during the day-time.

The second path, stretches 2450 km, from Heiss Island to St. Petersburg. The midpoint is located at geomagnetic latitude $\Phi'$=66°, normally in the auroral oval. This path is transauroral as the receiver, St. Petersburg, is situated at middle latitudes, and the transmitter, Heiss Island, is situated inside the polar cap. According to Pirog (2000), there is a high possibility for the appearance of the sporadic $E_{sr}$ layers (retardation type of sporadic E) on this path. However, there is a very low probability of encountering one-hop reflections of HF signals from the E-layer on this path, because the one-hop propagation via E-layer is possible only up to 2000 km, whereas the length of the path is 2450 km.

The third path, stretches 1450 km, from Lovozero to Heiss Island. The midpoint is located on geomagnetic latitude $\Phi'$=69.5°, normally near the boundary between the auroral oval and polar cap area. The midpoint moves inside the polar cap during appreciable geomagnetic disturbances. The path appears to be polar-auroral, since its receiver, Lovozero, is located in the auroral zone, and the transmitter, Heiss Island, lies inside the polar cap.

An oblique swept-frequency (3.5–27.5 MHz) sounding was conducted every hour on each of the three paths. Two rdio-propagation parameters were determined at the receiver, the MOF (maximum observed frequency) and the LOF (lowest observed frequency). The MOF value characterizes either the ionospheric F- or E-layer state, depending on the region that reflects a signal at the time. The MOF is controlled by the maximum electron concentration of the reflection layer, its altitude, and the path length. The LOF value depends not only on the technical equipment of radio path (power, antenna etc.), but also on the absorption in the lower ionosphere (Lundborg et al., 1995).

## 3 Parameters of geomagnetic storms

The description above already says where the measurements were made. It is necessary to mention that geomagnetic storm manifestations in the ionosphere of this region can significantly differ from manifestations in other regions (Blagoveshchensky et al., 2001).

### 3.1 Table 1 description

Fourteen geomagnetic storms have been selected from a list of CEDAR, GEM and ISTP storms (see Table 1). These were selected to represent winter, and equinox. The principal characteristics of the storms are presented in Table 1. The second column indicates the date of the storm and its strength according to Gonzales et al. (1994), using their classification system: intense storms are those with peak $D_{st}$ of $-100$ nT or less, moderate storms fall between $-50$ nT and $-100$ nT, and weak storms are those between $-30$ nT and $-50$ nT. The third column specifies which of these storms were associated with international research programs: Coupling, Energetics and Dynamics of Atmospheric Regions (CEDAR), CEDAR Storm Study (CSS), Geospace Environment Modeling (GEM), International Solar Terrestrial Physics (ISTP). Also, in Table 1, the following points are represented: the time of the onset of the expansive phase, $T_o$; the end time of the expansion phase $T_e$ ($T_e$ is defined later); and the storm duration $\tau$=$T_e - T_o$, in hours. Examples are shown in Figs. 2–5. Values of $\tau_o$ and $\tau_e$ are durations, in hours, of broadening of the range $\Delta$=MOF−LOF before the To and accordingly after $T_e$ (see Fig. 2). The MOF or LOF changes are determined relative to the monthly median values. The $AE_{max}$ and $D_{stm}$ levels are the maximum values of AE and $D_{st}$-indexes for the period of a storm. The parameter $A_{max}$ is the maximum absorption determined from the Sodankyla riometer, an instrument in the vicinity of the radio propagation paths (see

**Table 1.** List of geomagnetic storms considered (definition of the various parameters are given in Table 2).

| No | Date | Belonging | $T_o \div T_e$ UT, h | $\tau$, h | $\tau_o$,h | $\tau_e$,h | $AE_{max}$ nT $D_{stm}$ | $A_{max}$ dB | $t_{des}$, h | Radio path |
|---|---|---|---|---|---|---|---|---|---|---|
| 1 | 10 Jan 1997 moderate | CEDAR(CSS) ISTP | 06÷21 n | 15 | 2 | 6 | 1900 –80 | 5,8 | 2 | St. Pet-Heiss |
| 2 | 28–29 Mar 1997 moderate | ISTP | 15÷01 d | 10 | 3 | n/dabsr | 1400 –62 | 4,0 | 6 | St. Pet-Heiss |
| 3 | 10–11 Apr 1997 moderate | CEDAR(CSS) ISTP | 20÷08 d | 12 | 4 | 2 | 1200 –80 | 5,7 | 10 | St. Pet-Heiss |
| 4 | 15 May 1997 intense | GEM | 06÷16 n | 10 | 3,5 | 5 | 1100 –115 | 5,7 | 2 | St. Pet-Heiss |
| 5 | 27–28 Sep 1997 weak | ISTP | 15÷18 d | 27 | 4 | 4 | 1100 –43 | 6,5 | 5 | St. Pet-Heiss |
| 6 | 1 Oct 1997 intense | ISTP | 09÷20 n | 11 | 2 | 2 | 1600 –101 | 5,8 | 1 | St. Pet-Heiss |
| 7 | 5 Nov 97 weak | ISTP | 08÷18 n | 10 | 2 | n/d absr | 900 –44 | 1,0 | 4 | St. Pet-Heiss |
| 8 | 6–7 Jan 1998 moderate | ISTP | 16,5÷ d 13 | 20,5 | 2 | 5 | 1000 –78 | 3,0 | 8 | St. Pet-Heiss |
| 9 | 20–21 Jan 1998 weak | ISTP | 14,5÷ d 10 | 19,5 | 3,5 | 4 | 800 –30 | 2,0 | 4 | St. Pet-Heiss |
| 10 | 25 Mar 1998 moderate | GEM | 11÷20 n | 9 | 2 | n/d absr | 1000 –55 | 1,1 | 4 | St. Pet-Heiss |
| | 26 Mar 1998 weak | GEM | 12÷20 n | 8 | 2 | n/d absr | 900 –35 | 1,7 | 2 | St. Pet-Heiss |
| 11 | 25 Mar 1998 moderate | GEM | 11÷20 n | 9 | 2,5 | 3,5 | 1000 –55 | 1,1 | 0 | St. Pet-Lovoz |
| | 26 Mar 1998 weak | GEM | 12÷20 n | 8 | 2 | 1 | 900 –35 | 1,7 | 1 | St. Pet-Lovoz |
| 12 | 25 Mar 1998 moderate | GEM | 11÷20 n | 9 | 4 | 2 | 1000 –55 | 1,1 | 0 | Lovoz-Heiss |
| | 26 Mar 1998 weak | GEM | 12÷20 n | 8 | 1 | n/d | 900 –35 | 1,7 | 0 | Lovoz-Heiss |
| 13 | 17 Apr 1998 weak | ISTP | 03÷21 n | 18 | 3 | 3 | 800 –30 | 0,6 | 4 | St. Pet-Heiss |
| 14 | 17 Apr 1998 weak | ISTP | 03÷21 n | 18 | 0 | 2 | 800 –30 | 0,6 | 3 | St. Pet-Lovoz |
| 15 | 17 Apr 1998 weak | ISTP | 03÷21 n | 18 | 0 | 3 | 800 –30 | 0,6 | 0 | Lovoz-Heiss |
| 16 | 2–3 May 1998 moderate | ISTP | 05÷11 n | 30 | 2 | n/d | 1700 –80 | 3,6 | n/d | St. Pet-Lovoz |
| 17 | 24–25 Sep 1998 intense | GEM ISTP | 20÷17 d | 21 | 4 | 3 | 2000 –205 | 5,0 | 11 | St. Pet-Heiss |
| 18 | 12–13 May 1999 weak | ISTP | 18÷17 d | 23 | 4 | 3 | 1300 –49 | 2,0 | 0 | St. Pet-Heiss |

Figs. 1, 2). The parameter $t_{des}$ is the total number of hours in the interval $\tau$, during which there are no observed signals at the receiving point due to high absorption. During $t_{des}$, the above-the-MUF conditions are most likely to be absent. The last column of Table 1 shows the path investigated for each storm. Other designations in the table are: n/d – no data, absr – absorption, n – night, d – day-time.

The AE-index was chosen to estimate the storm intensity. The $D_{st}$-index is presented in Table 1 for completeness. However, although the AE-index is not ideal for the world storm description (Gonzales et al., 1994), it is preferable here since it has a higher time resolution.

The value A, dB estimates the intensity of absorption shown by the riometer data, at 30 MHz, by Sodankyla station,

**Table 2.** Definitions used in the paper and Table 1.

| Parameter | Definition |
|---|---|
| MOF, MHz | The maximum observed frequency |
| LOF, MHz | The lowest observed frequency |
| $\Delta$=MOF-LOF, MHz | The frequency range |
| $T_o$, h | The moment of storm expansion phase onset |
| $T_e$, h | The moment of storm expansion phase end |
| $\tau=T_e-T_o$, h | Storm expansion phase duration |
| $\tau_o$, h | Duration of broadening of the range $\Delta$ before $T_o$ |
| $\tau_e$, h | Duration of broadening of the range $\Delta$ after $T_e$ |
| $t_{\mathrm{des}}$, h | Total number of hours in the interval $\tau$, during which there is no propagation |
| $A_{\mathrm{max}}$, dB | The maximum level of Sodankyla riometer absorption |
| $AE_{\mathrm{max}}$, nT | The maximum value of AE-index for the period of storm |
| $D_{stm}$, nT | The minimum value of $D_{st}$-index for the period of storm |

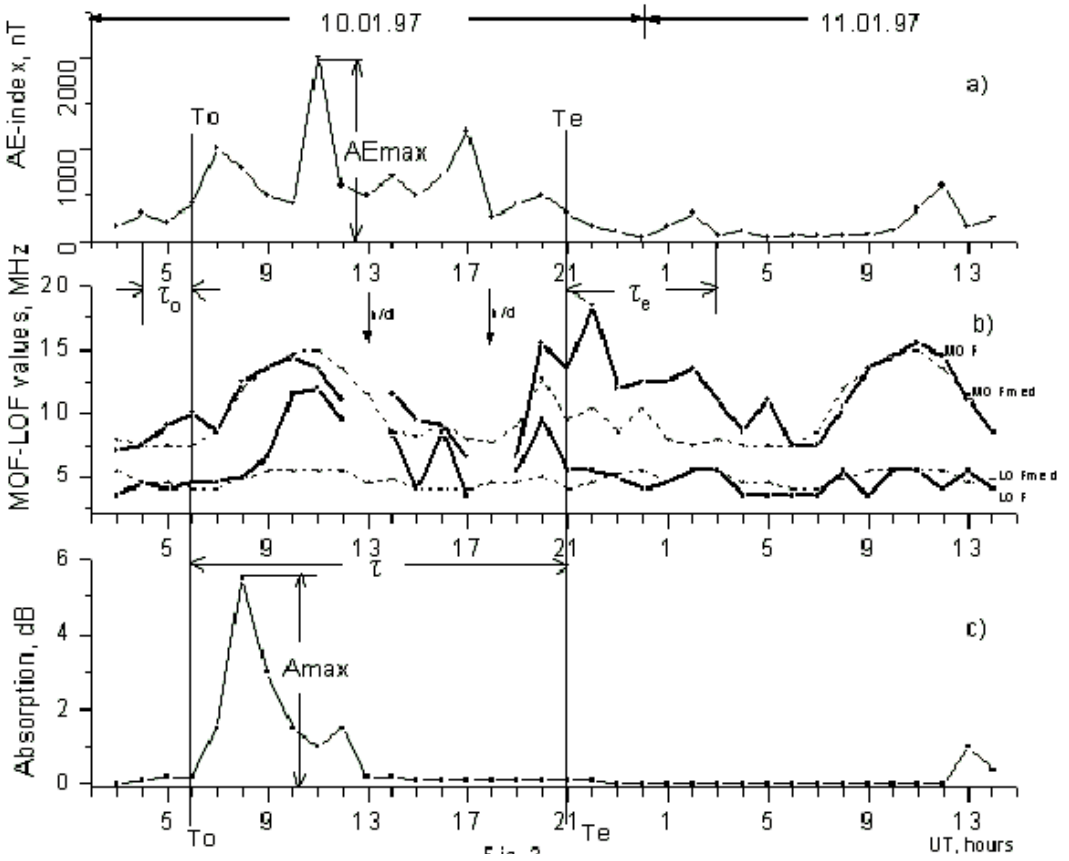


**Fig. 2.** Variations of the AE-index **(a)**, MOF and LOF values on the St. Petersburg-Heiss Island path **(b)** and absorption level A by Sodankyla riometer **(c)** during a storm of 10–11 January 1997. Absent of propagation is shown by arrows. Dashed lines are median values.

Finland. This station is situated close, but not exactly, on the paths used in the study, Fig. 1. Nevertheless, the estimation of absorption here is approximate, and more likely has qualitative characteristics rather than quantitative ones.

A list of the various parameters used for this study are presented in Table 2.

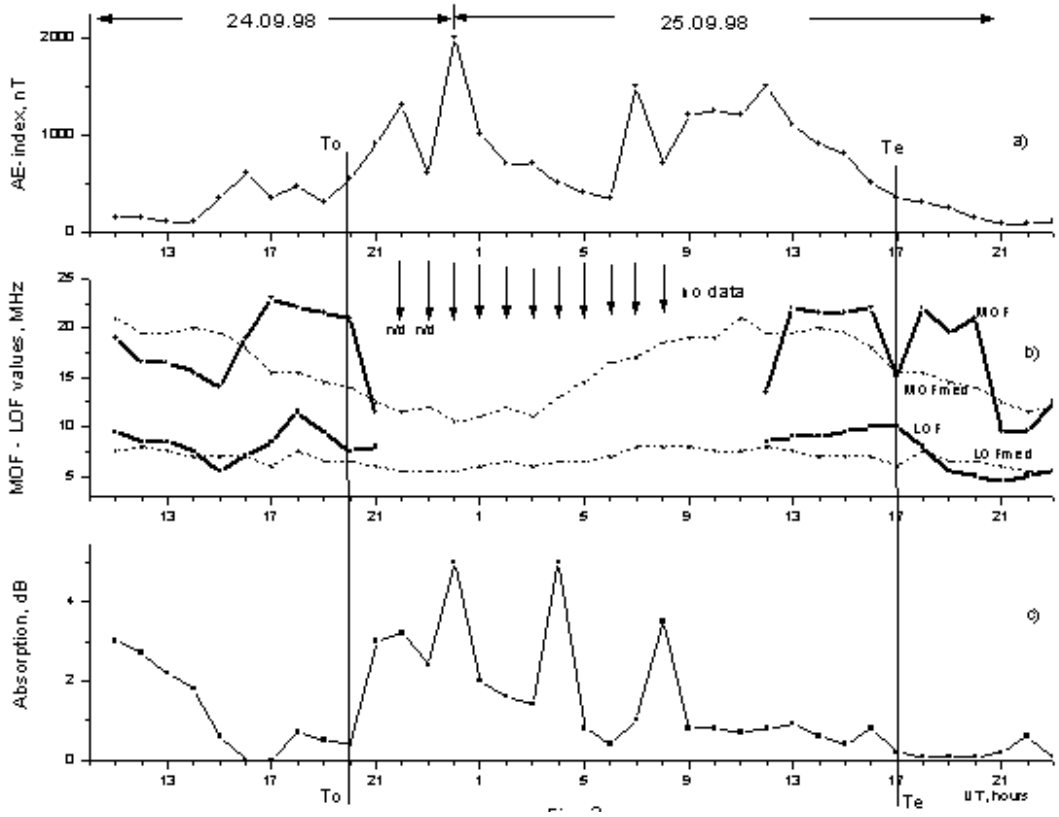


**Fig. 3.** The same as in Fig. 2 but for an intense storm of 24 September 1998.

### 3.2 Selection of $T_o$ (storm expansion phase onset)

All the storms differ from each other by their time-histories in AE-indexes. Storms can arise on a quiet AE background, e.g. storms numbers 1 (Fig. 2), 3, and 7 (Table 1), a moderate background, e.g. numbers 2, 8, 9, and 16, or a disturbed background, e.g. numbers 4, and 17 (Fig. 3). Also storms may develop after a single substorms, e.g. 5, 6, and 18 (Fig. 4). The evolution of each magnetospheric storm is different. There can be slow growth of the AE-index, as exhibited by storm numbers 3, 17, and 18 (Figs. 3, 4); moderate growth, like numbers 1 (Fig. 2) and 7; rapid growth, like numbers 4, 6, 8, 9, and 16; and very rapid growth, like number 5, with an $AE_{max} \geq$ 1500–2000 nT. The storm expansion phase onset, as with the time of sudden growth of AE-index, does not depend on the latitude, longitude, year, or month, and may occur at any time of a day, (Table 1). In this study, the threshold, which has to be crossed by the increasing AE-index before the disturbance maximum, is $AE_{limit}$=300–500 nT (see Figs. 2–5). In terms of the value of the storm's character and considering the analysis of $D_{st}$ and $B_z$, this $AE_{limit}$ value was determined primarily from the observed AE range, and using this the $T_o$ moment was selected with an accuracy of $\sim$1 h.

### 3.3 Selection of $T_e$ (storm expansion phase end)

Besides the factors mentioned above in Sect. 3.2, there is an additional complicating factor. According to observational data, at the end of the disturbance, when the AE-index is diminishing, significant riometer absorption in the ionosphere sometimes takes place. This effect is demonstrated by storms numbers 18 and 12, Figs. 4, 5, and 6. The threshold of $AE_{limit} \leq$100–300 nT, and for ionospheric absorption A$\leq$0.5–0.6 dB, designates approximately the choice of the $T_e$ moment. Estimates that are more accurate than $\pm$1 h are difficult.

Figures 2–6 (panel a) illustrate AE-variations, MOF and LOF variations (panel b), and variations of the absorption level A, measured by Sodankyla station (panel c) for the periods of the selected storms. Thus, Figs. 2–4 are "representative" of each of the three years 1997, 1998 and 1999, respectively for the St. Petersburg-Heiss Island path. Figures 5 and 6 display the data for the St. Petersburg-Lovozero and Lovozero-Heiss Island paths, respectively.

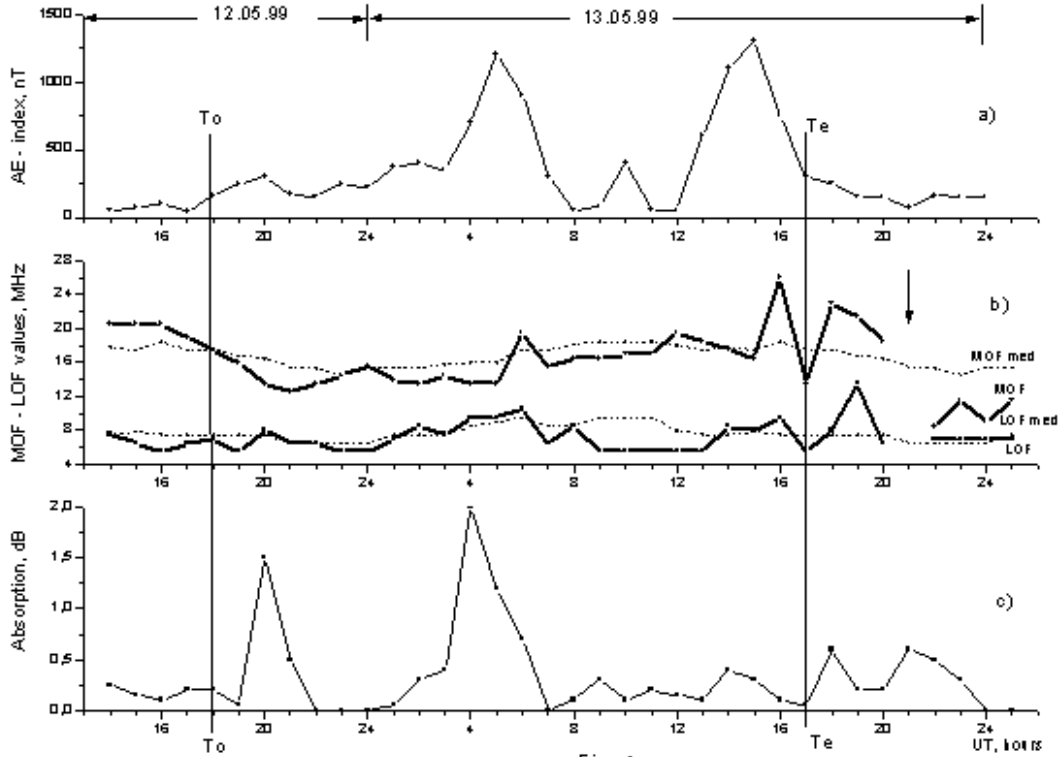


**Fig. 4.** The same as in Fig. 2 but for a weak storm of 12–13 May 1999.

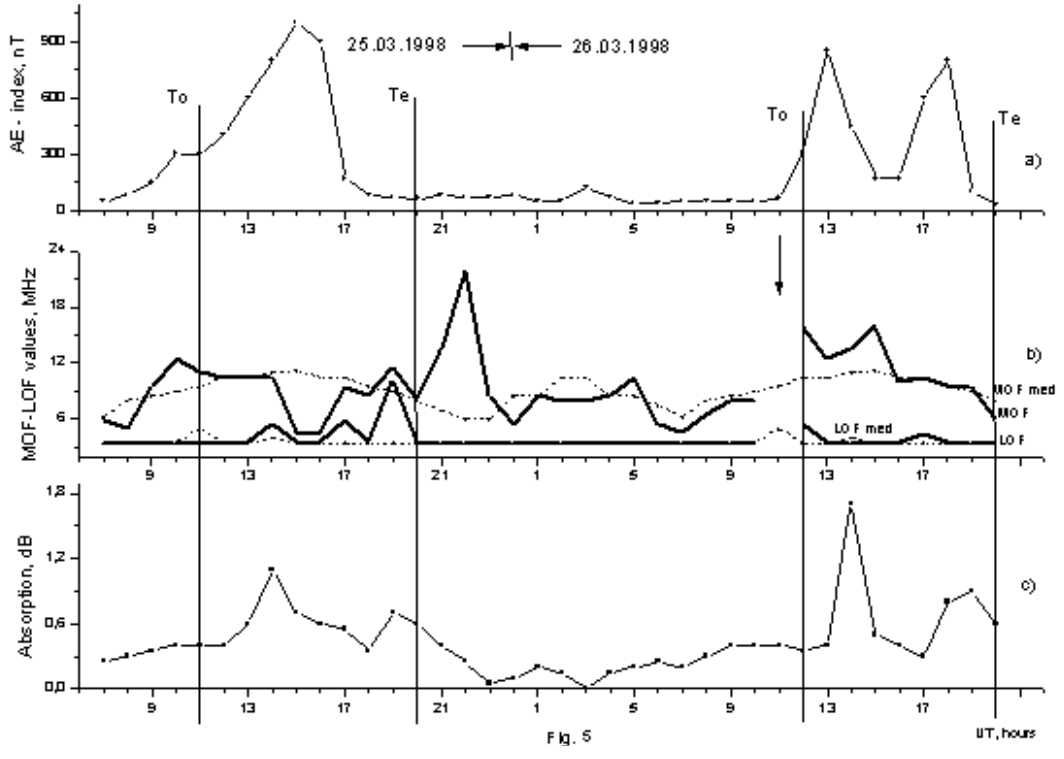


**Fig. 5.** The same as in Fig. 2 but for the St. Petersburg-Lovozero path and two storms of 25–26 March 1998.

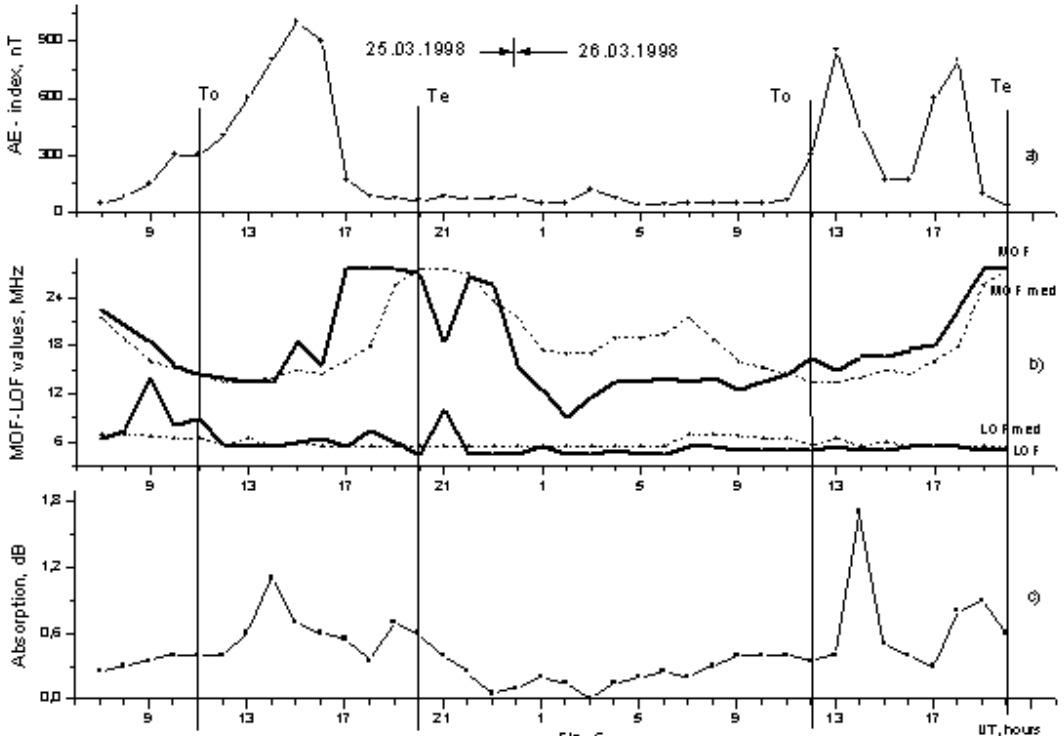


**Fig. 6.** The same as in Fig. 5 but for the Lovozero-Heiss Island path.

## 4 Data discussion

### 4.1 Table 1 data analysis

There is no obvious relationship between the $AE_{max}$ values and $\tau$, $\tau_o$ and $\tau_e$ values. Analysis shows that on the St. Petersburg-Heiss Island path, where the statistics are the greatest, the median value is $\tau_o$=3.5 h, for day-time *d-storms* (numbers 2, 3, 5, 8, 9, 17, and 18). While for night-time *n-storms* (numbers 1, 4, 6, 7, 10, and 13) the median value is $\tau_o$=2.4 h. This result is explained physically by the presence of energetic particle precipitation in the cusp and auroral zone in the day-time before a storm (Gulielmi et al., 2001), which ionizes the ionospheric F2-layer for a longer time, $\tau_o$=3.5 h, than at night, $\tau_o$=2.4 h, when precipitation occurs from the night-side of the plasma ring (auroral peak).

The time of the path outage, $t_{des}$ (the interval of propagation failure), for the St. Petersburg-Heiss Island path (Table 1) depends on the LT or on the location of the path relative to the auroral absorption area. The median values of $t_{des}$ and $\tau$ are 6 h, and 20 h, respectively, for day-time storms. The corresponding values for night-time storms are 2 h, and 10 h. The average percentage of loss of propagation path within the interval $\tau=T_e-T_o$, is 30% (6/20) for all day-time storms and 20% (2/10) for all night-time storms. Thus, there is a significant difference between day- and night-time behaviour.

If the radio signal is absorbed, its absence is called a failure. This observation is valid for a number of storms, namely 10, 11, 12. 13, 14, and 15. The Lovozero-Heiss Island path has no failures, because the path is situated mainly outside the region suffering from auroral absorption.

### 4.2 The main effect on MOF

The AE-index shows that for most storms there are large fluctuations in AE (see Figs. 2–6, panels a for example). The time interval between peaks in such data is about 3–7 h, indicating that there most storms comprise a series of substorms (Gonzales et al., 1994). We will adhere to this standpoint, though it is known that a storm is not necessarily a set of substorms. Blagoveshchensky et al. (1992, 1996, 2000) and Blagoveshchensky and Borisova (2000) have considered substorm effect on the ionosphere which is called the main effect (ME). They suggest that there are three main components that affect the variations of ionospheric parameters. These are:

Step 1. During the growth phase of the substorm, there is an increase in *fo*F2 values and a decrease in *hm*F2 values, with respect to the quiet median value, about 4 h before $T_o$, and lasting 2–3 h (Blagoveshchensky et al., 2006).

Step 2. During the expansion phase, *fo*F2 falls, and *hm*F2 rises with respect to the median value immediately following $T_o$, until close to $T_e$.

Step 3. A repeat of step 1 phenomena occurs during the substorm recovery phase, after $T_e$.

It must be emphasized that the ME behaviour applies to the F2 layer of the ionosphere. In the lower ionosphere, the regularities are essentially different. However, in this paper, we consider the features of ionospheric radio propagation during storms/substorms. The object of this study is to study variations of the frequency range $\Delta$=MOF−LOF under disturbed conditions. Here the MOF value is a proxy of *fo*F2. However, LOF depends on both the ionization density of the lower ionosphere and the technical equipment that is used. Therefore, the ME impact can be considered only for MOF.

Our observational data from storms reveal that MOF variations from the F2-layer show the main effects during separate substorms that comprise the storm. For example on 12–13 May 1999 (Fig. 4), the MOF peak within 4 h of the start of the storm (∼13:00 UT) and lasts about 5 h. During the first AE-maximum, from 18:00 to 22:00 UT, there is a decrease of MOF values below the median, which is the second step of ME. From 22:00 to 01:00 UT, after the end of the first substorm, the rise of MOF occurs, which is the third step of ME. As with the first substorm, a rise precedes the second substorm, from 01:00 to 06:00 UT, which is the second step of ME. At the end of the second substorm, there is a positive MOF peak, from 05:00 till 07:00 UT, which is third step of ME. The positive peak of MOF occurs again before the third substorm, from 11:00 to 14:00 UT, step one of ME. Then MOF decrease, from 14:00 till 15:00 UT (step 2 of ME), and then it rises once more from 15:00 up to 17:00 UT, step 3 of ME. The timing of MOF variations depends on the time interval between AE-peaks and their intensity. Intense peaks are associated with significant growth of absorption and hence signal loss, as one can see in Fig. 3, from 22:00 UT through to 11:00 UT.

### 4.3 Physical mechanisms of MOF variations

#### 4.3.1 Analysis of the first step of ME before a storm when F2MOF (or $\Delta$*fo*F2) grows during $\tau_o$

A magnetospheric disturbance is formed as a result of interaction between the magnetosphere and the plasma flow of solar wind. There is normally a sudden magnetic impulse (SI) or a storm sudden commencement (SSC) when the front of an interplanetary solar shock wave contacts the terrestrial magnetosphere. A compression of the magnetosphere occurs. This compression results in the generation of electromagnetic waves, such as Pc1. The location of the origin region of Pc1 is associated with the location of the plasmapause (Pudovkin et al., 1976). According to papers of Gulielmi et al. (2001) and Kangas et al. (2001), Pc1 can begin not only after SI, but also before it. The mechanism is that before the shock waves propagating in non-collision solar wind plasma, there are so-called pre- shock areas. An example of this area may be the plasma-wave turbulence formed in front of the near Earth shock wave, or turbulence before an interplanetary shock wave. The latter turbulence will affect the magnetosphere some time before the moment of SI formation, causing Pc1 waves. Kangas et al. (2001) suggest that these Pc1 pulsations, observed before SSC, as the manifestations of impacts of the interplanetary pre- shock area (upstream) on the geomagnetic field.

Another phenomenon created by interplanetary pre-shock areas is beams of the particles reflected from the shock front and those traveling from the Sun with speeds higher than the speed of a shock. These accelerated solar wind particles precipitate into the Earth's ionosphere, causing the following geophysical effects: additional ionization, heating, and increased absorption some hours before the SI. The ionospheric projection of the cusp should be the most probable location of the precipitation. The auroral oval is another region of possible precipitation from the entry sheet of the magnetosphere. These effects of ionization, heating, and absorption may be considered as ionospheric forerunners of SI.

Gulielmi et al. (2001) provide significant evidence of enhanced riometer absorption occurring up to 3 h before an SI using data from Sodankyla. At this time Sodankyla was considered to be equatorward of the cusp. The cause of absorption is an intensification of flow of reflected particles, moving before the flash flow front.

Danilov et al. (1985) proposes the different formation mechanism for the positive phase of an ionospheric storm, before the beginning of a magnetic disturbance (first step of ME before a storm, during $\tau_o$). Precipitation of accelerated particles occurs during the day, in the diurnal cusp region, causing heating of the ionospheric F2-layer. This in turn causes disturbed neutral winds equatorward of the cusp which results in the transfer of thermospheric gas with a large O/N2 ratio. This reduces the loss rate and leads to the intensification of F-layer ionization. Under conditions prior to the beginning of a magnetic storm, the growth of ionization will cause, in a unique manner, the positive ionospheric disturbance in the evening and at night. This behaviour is confirmed by experiments (Ondoh and Obu, 1980): (i) there is a growth of electron density in the cusp region; and (ii) positive *fo*F2-deviations are frequently observed some hours before the magnetic disturbance. These positive $\Delta$*fo*F2 values are related to the particle precipitation inside the cusp area before the storm-related auroral precipitation, and the development of ring current, which is considered to be the start of magnetic disturbance (Gonzales et al., 1994). Precipitation inside the cusp area is related to regions of the magnetosphere such as the low latitude boundary layer, whereas the currents, which cause Joule-heating of the ionospheric E-layer, are related to other magnetospheric regions (magnetosphere tail, plasma sheet, field-aligned currents). Hence, these factors explain why the positive phase of the ionospheric storm, before the beginning of a magnetic disturbance, is possible.

We now consider the main mechanisms:

*Day-time conditions*

There are several possible mechanisms of F2MOF increase ($\Delta foF2>0$) within $\tau_o$=3.5 h before the beginning of the magnetic disturbance.

1. The growth of $\Delta foF2$ values at high- and mid-latitudes before the storm is a result of lifting the F2-layer or *hm*F2 by action of the vertical drift. The vertical drift is caused by, firstly, the occurrence of electric fields, and, second, due to meridional southward winds (Buonsanto, 1999; Danilov and Morozova, 1991). These winds play a dominant role here.

2. Particle precipitation from the plasmasphere due to its compression, as a result of magnetosphere compression, may be another source of ionization increase (Park, 1974). These particles ionize the F2-layer of the ionosphere. The most probable area of particle precipitation is located from mid-latitudes, up to $\Phi_L \sim 70°$, with a maximum at latitude $\Phi_L \sim 50°$ (Lastovicka, 2002; Chao-Song and Foster, 2002).

*Night conditions*

There are also several possible mechanisms of F2MOF growth ($\Delta foF2>0$) within $\tau_o$=2.4 h.

1. The drift of thermospheric gas from the diurnal cusp through the pole to the night-side. This mechanism, according to (Lastovicka, 2002), leads to the increase of ionization and positive values of $\Delta foF2$.

2. Effects of electric fields impact (Chao-Song and Foster, 2002). In particular, electric fields can penetrate at the night-side.

3. Enhanced fluxes of cold plasma from the plasmasphere, which can cause the increase of $\Delta foF2$ in the hours before sunrise (Danilov and Morozova, 1991).

4. Particle precipitation from the magnetosphere tail, specifically from the plasma sheet, due to compression of the magnetosphere, before SSC. Additionally to positive $\Delta foF2$, this mechanism causes the sporadic Esr-layers formation at high latitudes, several hours before $T_o$ (Pirog et al., 2000).

The relative importance of these mechanisms will vary between individual storms.

#### 4.3.2 Analysis of the second step of ME during a storm, when F2MOF (or $\Delta foF2$) falls within $\tau$

In the case of positive disturbance, accompanied by a negative one, the ionospheric storm phenomenon turns out to be related to two widely different magnetospheric regions, and to widely different paths of penetration of solar wind energy into the polar ionosphere. For example, as was described above, there is a path, associated with a particle precipitation in the diurnal cusp and ionospheric heating inside the cusp at F-layer altitudes. This causes positive ionospheric disturbances at night ($\Delta foF2>0$). Another mechanism, related to Joule-heating in the E-layer (magnetospheric tail, plasma sheet etc.), causes negative ionospheric disturbances ($\Delta foF2<0$) at night. A redistribution of ionization happens here during the storm, due to heating during the expansion phase: the electron density in the F2-layer falls and it rises in E-layer (Blagoveshchensky et al., 1996).

Another cause, particle precipitation, is also possible. The intensity and severity of auroral flows increase after $T_o$. Diffuse precipitation of the low energy electrons becomes stronger, while a disturbance develops. This leads to ionization increase at lower altitudes: first in the E-region, then in the D-layer.

#### 4.3.3 Analysis of the third step of ME at the end of a storm, when F2MOF ($\Delta foF2$) grows within $\tau_e$

The F2MOF ($\Delta foF2$) rise during the recovery phase of a storm may be caused by ring current effects. During this phase, there is a decrease of the electric field of convection (Buonsanto, 1999), and the plasmapause (the outer boundary of the region of plasma of ionospheric origin) expands, due to filling up the plasmasphere with ionized particles. According to Buonsanto (1999), the penetration of some energy in the upper atmosphere can come from the magnetospheric ring current. Coulomb collision between ring current ions and electrons provides the heating, which flows down to the ionosphere, and is a cause of the stable auroral red arcs (Kozyra et al., 1984). Tinsley (1979) also shows that the energy transfer from ring current particles to neutrals generates energetic neutral atoms that are not affected by the magnetic field; therefore, they can influence the upper atmosphere at any latitude.

### 4.4 Frequency range variations

Figures 2–6 demonstrate the features of frequency range $\Delta$=MOF−LOF behavior. The first three figures show behaviour on the St. Petersburg-Heiss Island path.

Figure 2 displays data for the storm on 10–11 January 1997, which evolves on a quiet background. This storm is a moderate one, because $D_{stm}$=−80 nT and AE shows a modest increase. For about 2 h before $T_o$, there is broadening of the frequency range $\Delta$=MOF−LOF. Directly after $T_o$ ($AE_{limit}$=400 nT), the absorption in the ionosphere increases dramatically or significantly. The LOF maximum (11UT) arises with a delay of 3 h. The absorption maximum, $A_{max}$=5.8 dB is at 08:00 UT. At this time, the MOF-LOF range becomes very narrow, until $T_e$ (21:00 UT),

thereafter it expands over the next 6 h interval from 21:00 to 03:00 UT. Hereafter MOF and LOF values return to their median values. MOF and LOF data are absent at 13:00 UT and 18:00 UT, which is probably due to absorption.

Figure 3 illustrates the data for the intense storm on 24 September 1998, which evolves from the disturbed background, of a preceding substorm, and is characterized by a slow rise in the AE-index. Here the MOF-LOF range expansion before To occurs from 16:00 till 20:00 UT, $\tau_o$=4 h. The main phase of the storm is between ~22:00 UT and ~11:00 UT, the MOF-LOF range is narrow, with periods of the intensive ionospheric absorption, $A_{max}$=5.0 dB, causing loss of radio propagation. After $T_e$, from 17:00 to 20:00 UT, $\tau_e$=3 h, the MOF-LOF range is expanded. This MOF behaviour is similar to the $\delta$TEC behaviour seen by the GPS network (Afraimovich et al., 2001).

The weak storm on 12–13 May 1999 (Fig. 4), evolves from a weakly disturbed background, with a preceding substorm. It has a slow increase in the AE-index. There is also range broadening of MOF-LOF before $T_o$ and after $T_e$, $\tau_o$=4 h and $\tau_e$=3 h. Range values are narrowed mostly during AE-index peaks from 19:00 to 22:00 UT, from 01:00 to 06:00 UT, and again from 13:00 to 15:00 UT. Data for 21:00 UT are absent. There is no signal loss during this weak storm during the interval $\tau$, because the absorption in the ionosphere is moderate, with a maximum value $A_{max}$=2.0 dB.

Figure 5 illustrates variations of the frequency range on the St. Petersburg-Lovozero path. There are two storms, a moderate one with one maximum (11:00–20:00 UT), and a weak one with two maxima between 12:00 and 20:00 UT. Broadening of the MOF-LOF range can be seen before and after the storms, with a narrowing of the range during a storm, when value of the AE-index is at its maximum. The St. Petersburg-Lovozero path is located close to mid-latitudes, therefore MOF-LOF variations here show the same characteristics as the storms described above. However on this occasion a different behaviour is observed on the high-latitude Lovozero-Heiss Island path.

Figure 6 shows that the Lovozero-Heiss Island path is dominated by propagation via Es-layers. There are MOF-LOF range broadenings at the onset and the end of a storm in Fig. 6, but they are insignificant with respect to the median value. A narrowing of the range during a storm does not occur at all. Signal absorption does not play an essential role on this path, since this path is located almost entirely inside the polar cap area poleward of the auroral absorption region. The HF radio propagation is most stable here, because its susceptibility to storm effects is minimal.

## 5 Conclusions

1. A number of CEDAR, GEM and ISTP storms have been investigated, and some general behaviour patterns have been determined. The main result is that the range of MOF-LOF frequencies extends several hours before the beginning of a storm, sharply narrows during a storm, and extends again within several hours after the end of the storm. Also the same three characteristics are observed for individual substorms. This statement refers to paths whose midpoints are situated at geomagnetic latitudes $\Phi'$=61° and 66°. At higher latitudes ($\Phi'$=69.5°) the patterns are less clear. There is also a close relationship of the LOF values and riometer absorption A, and signal loss due to high absorption during intense disturbances.

2. The discovery of this regular behaviour represents the novel component of this study and should be useful for radio propagation prediction and frequency management at high latitudes.

3. Variations of F2MOF (when the signal is reflected from F2-layer) represent the combination of main effects (ME) of separate substorms, of which most storms consist. The main effect represents the positive $\Delta fo$F2 values within several hours before $T_o$, negative $\Delta fo$F2 within the interval $T_o - T_e$, and positive $\Delta fo$F2 again, within several hours after $T_e$ moment. The total, rather complex, picture of a storm depends on the time intervals between AE peaks, and the AE intensities.

4. Variations of the riometer absorption A and AE-index are basically similar during less intense storms, though sometimes delayed peaks of absorption A are observed, compared with peaks of the AE-indexes. The peaks of absorption A and minima of LOF values often coincide. Hence, LOF values are defined mainly by absorption in the lower ionosphere.

5. The Es-layer manifestations, giving high MOF values during the disturbances, are greatest on Lovozero-Heiss Island path with the midpoint at $\Phi'$=69.5°. The Es-layer usually screens the F-layer. Absorption on this path is minimum, and signal loss is absent.

6. Two main phenomena (i) ionization increase in the F2 layer (positive $\Delta fo$F2) several hours before $T_o$ and (ii) dramatic increase of riometer absorption at the beginning of development of the storm expansion phase may be considered as forerunners of the storm expansion phase. Particles, precipitating inside the cusp and auroral zone before the storm, ionize the ionospheric F2-layer for a longer interval ($\tau_o$=3.5 h) in the day-time than in the night-time ($\tau_o$=2.4 h) when precipitation occurs from the night side of plasma ring (auroral peak).

7. The St. Petersburg- Heiss Island radio path has a time-interval of destroyed path $t_{des}$ (interval of signal loss) that depends on the local time LT. The median value of $t_{des}$ is 6 h, and median value of $\tau$ is 20 h for the day-time storms. For the night-time storms, the median value $t_{des}$

is 2 h, and the median value of $\tau$ is 10 h. The average percent of path destruction during the storm in the interval $\tau = T_e - T_o$ is 6/20=30% for all day-time storms and 2/10=20% for all night-time storms. Thus, firstly, duration of storms is longer during the day than during the night, and, secondly, during disturbances the path is destroyed for longer in the day-time than at the night.

8. In spite of the established behaviour of such parameters as the MOF, LOF, A and AE during a magnetospheric storm, there are some storm events ($\leq$5%) which do not comply with the general tendencies.

9. Space weather during the intensive magnetospheric storms crucially changes the processes in the magnetosphere and ionosphere. According to the present study at high latitudes there exists not only the traditional mechanism of solar energy transfer into the upper atmosphere through the magnetosphere tail, plasma sheet and auroral ionosphere but the other, little-known mechanism: through the diurnal cusp and the entry sheet of magnetosphere.

*Acknowledgements.* The authors of the paper would like to thank Alan Rodger for useful discussion as well as NASA (USA), Kyoto (Japan) and Sodankyla (Finland) services providing scientific data that have been used in this study.

Topical Editor M. Pinnock thanks two anonymous referees for their help in evaluating this paper.

## References

Afraimovich, E. L., Kosogorov, E. A., Leonovich, L. A., and Pirog, O. M.: A global picture of large-scale disturbances during the September 25, 1998 as deduced from GPS data, Res. Geomagn., Aeron. Space-Phys., Siberian Branch of RAS, Irkutsk, 112, 142–156, 2001 (in Russian).

Baker, D. N.: Solar wind-magnetosphere drivers of space weather, J. Atmos. Space-Phys., 58(11), 1509–1526, 1996.

Blagoveshchensky, D. V. and Borisova, T. D.: Substorm effects of ionosphere and HF propagation, Radio Sci., 35(5), 1165–1171, 2000.

Blagoveshchensky, D. V., Borisova, T. D., and Egorova, L. V.: Pre- and after substorm situations in the ionosphere and decameter radio wave propagation, Geomagn. Aeron., 36(4), 125–134, 1996 (in Russian).

Blagoveshchensky, D. V., Egorova, L. V., and Lukashkin, V. M.: High-latitude ionospheric phenomena diagnostics by high-frequency radio wave propagation observations, Radio Sci., 27(2), 267–274, 1992.

Blagoveshchensky, D. V., Maltseva, O. A., and Rodger, A. S.: Ionosphere dynamics over Europe and western Asia during magnetospheric substorms 1998–99, Ann. Geophys., 21, 1141–1151, 2003, http://www.ann-geophys.net/21/1141/2003/.

Blagoveshchensky, D. V., MacDougall, J. W., and Piatkova, A. V.: Ionospheric effects preceding the October 2003 Halloween storm, J. Atmos. Space-Phys., 68, 821–831, 2006.

Blagoveshchensky, D. V., Pirog, O. M., Polekh, N. M., and Chistyakova, L. V.: Mid-latitude effects of the May 15, 1997 magnetic storm, J. Atmos. Space-Phys., 65, 303–310, 2003.

Buonsanto, M. J.: Ionospheric storms – a review, Space Sci. Rev., 88, 563–601, 1999.

Chao-Song Huang and Foster, J. C.: Prompt effects of solar wind variations on the inner magnetosphere and midlatitude ionosphere, Space Weather Week, April 16–19, Boulder, Colorado, Abstracts, p. 17, 2002.

Danilov, A. D. and Morozova, L. D.: Thermosphere-ionosphere interaction during ionospheric storms (review), Geomagn. Aeronom., 31(2), 209–222, 1991 (in Russian).

Danilov, A. D., Morozova, L. D., and Mirmovich, E. G.: About a possible nature of the positive phase of ionospheric storms, Geomagn. Aeronom., 25(5), 768–772, 1985 (in Russian).

Galeyev, A. A., Galperin, Yu. I., and Zeliony, L. M.: The project "Interball" by the solar–terrestrial physics investigations, Cosmic Studies, 34(4), 339–362, 1996.

Gonzales, W. D., Joselyn, J. A. , Kamide, Y., et al.: What is a geomagnetic storm?, J. Geophys. Res., 99(A4), 5771–5792, 1994.

Goodman, J. M. and Ballard, J. W.: An examination of elevated frequency propagation over a transpolar path, Radio Sci., 39, RSIS29, doi:10.1029/2002RS002850, 2004.

Gulielmi. A. V., Zolotukhina, N. A., Kangas, J., et al.: The build-up of Pc1 wave activity prior to sudden magnetic impulses SI, Res. Geomagn. Aeron. Space-Phys., Siberian Branch of RAS, Irkutsk, 112, 115–123, 2001 (in Russian).

Hunsucker, R. D. and Hargreaves, J. K.: The high-latitude ionosphere and its effects on radio propagation, Cambridge University Press, 2003.

Kangas, J., Kultima, J., Guglielmi, A., Potapov, A., and Hayashi, K.: Impact of interplanetary shock on the ULF wave activity: A case study of the storm sudden commencement on September 22, 1999, Earth Planets Space, 53, 1173–1182, 2001.

Kozyra, J. U., Chandler, M. O., Hamilton, D. C., Peterson, W. K., Klumpar, D. M., Slater, D. W., Buonsanto, M. J., and Carlson, H. C.: The role of ring current nose events in producing stable auroral red arc intensifications during the main phase: observations during the September 19-24, equinox transition study, J. Geophys. Res., 98, 9267–9283, 1984.

Lastovicka, J.: Monitoring and forecasting of ionospheric space weather – effects of geomagnetic storms, J. Atmos. Space-Phys., 64, 667–705, 2002.

Lundborg, B., Broms, M., and Derblom, H.: Oblique sounding of an auroral ionospheric HF chnnel, J. Atmos. Space-Phys., 57. 51–63, 1995.

Ondoh, T. and Obu, K.: Prediction of HF communications disturbances by pre-SC HF field increases on polar paths crossing the auroral zone, Solar-Terrestrial Prediction, Proc., 4, D21–30, 1980.

Park, C. G.: A morphological study of substorm-associated disturbances in the ionosphere, J. Geophys. Res., 79, 2821–2827, 1974.

Pirog, O. M., Urbanovich, V. D., and Zherebtsov, G. A.: Effects of substorms in the night auroral E-region, 5th International Conference on Substorms, St.-Petersburg, Book of abstracts, 545–547, 2000.

Pudovkin, M. I., Raspopov, O. M., and Kleimenova, N. G.: Disturbances of the Earth's electro-magnetic field, Chapter 2,

Leningrad State University, p. 270, 1976 (in Russian).
Tinsley, B. A.: Energetic neutral atom precipitation as a possible source of midlatitude F region winds, Geophys. Res. Lett., 6, 291–293, 1979.
Warrington, E. M. and Stocker, A. J.: Measurements of the Doppler and multipath spread of HF signals received over a path oriented along the midlatitude trouth, Radio Sci., 38(5), 1080, doi:10.1029/2002RS002815, 2003.